

Article

Transilient Response to Acetone Gas Using the Interlocking p+n Field-Effect Transistor Circuit

Xinyuan Zhou ^{1,2,3}, Jinxiao Wang ⁴, Zhou Wang ¹, Yuzhi Bian ^{1,2}, Ying Wang ¹, Ning Han ^{1,3,*} 
and Yunfa Chen ^{1,3,*}

- ¹ State Key Laboratory of Multiphase Complex Systems, Institute of Process Engineering, Chinese Academy of Sciences, Beijing 100190, China; zhouxinyuan14@mails.ucas.edu.cn (X.Z.); lovekeyanzhou@163.com (Z.W.); bianyuzhi17@mails.ucas.edu.cn (Y.B.); wangying@ipe.ac.cn (Y.W.)
- ² College of Chemical Engineering, University of Chinese Academy of Sciences, No. 19A Yuquan Road, Beijing 100049, China
- ³ Center for Excellence in Regional Atmospheric Environment, Institute of Urban Environment, Chinese Academy of Sciences, Xiamen 361021, China
- ⁴ College of Materials Science and Engineering, Xi'an Jiaotong University, Xi'an 710049, China; 13227885265@163.com
- * Correspondence: nhan@ipe.ac.cn (N.H.); chenylf@ipe.ac.cn (Y.C.); Tel.: +86-010-6255-8356 (N.H.)

Received: 7 May 2018; Accepted: 5 June 2018; Published: 12 June 2018



Abstract: Low concentration acetone gas detection is significantly important for diabetes diagnosis as 1.8–10 ppm of acetone exists in exhaled breath from diabetes patients. A new interlocking p+n field-effect transistor (FET) circuit has been proposed for Mn-doped ZnO nanoparticles (MZO) to detect the acetone gas at low concentration, especially close to 1.8 ppm. It is noteworthy that MZO in this interlocking amplification circuit shows a low voltage signal of <0.3 V to the acetone <2 ppm while it displays a transilient response with voltage signal >4.0 V to >2 ppm acetone. In other words, the response to acetone from 1 ppm to 2 ppm increases by ~1233%, which is competent to separate diabetic patients from healthy people. Moreover, the response to 2 ppm acetone is hardly influenced by high relative humidity of 85%. In the meanwhile, MZO in this interlocking circuit possesses a high acetone selectivity compared to formaldehyde, acetaldehyde, toluene and ethanol, suggesting a promising technology for the widespread qualitative screening of diabetes. Importantly, this interlocking circuit is also applicable to other types of metal oxide semiconductor gas sensors. The resistance jump of p- and n-FETs induced by the change of their gate voltages is deemed to make this interlocking circuit produce the transilient response.

Keywords: Mn-doped ZnO; transilient response; field-effect transistor; diabetes; metal oxide semiconductor sensor

1. Introduction

Breath analysis has attracted much attention because it is a noninvasive method [1,2] compared with blood analysis and endoscopy. Hundreds of species of volatile organic compounds (VOCs) are in the exhaled gas of humans [3,4]. The concentrations of some specific VOCs are associated with abnormal medical conditions, including breast cancer [5], liver disease [6], lung cancer [7,8], and diabetes [9,10]. Clinical data show the concentration of acetone in exhaled gas from diabetes patients is in excess of 1.8 ppm while it is 0.3–0.9 ppm for healthy people [11,12]. Thus, many technologies have been developed to detect acetone for diabetes diagnosis, such as the selected ion flow tube mass spectrometry (SIFT-MS) [13,14] and gas chromatography-mass spectrometry (GC-MS) [15,16]. However, the challenge to the widespread application of these technologies is their large instrument size, complex operation and time-consuming process.

On the other hand, gas sensors based on metal oxide semiconductors (MOX), such as WO_3 [17,18], In_2O_3 [19,20], SnO_2 [21] and ZnO [22–24], have become promising candidates due to their trend of miniaturization, easy fabrication, low cost and high integration potential in portable devices [25,26]. The Gd-doped WO_3 /reduced graphene oxide nanocomposite [17] displayed improved gas sensing properties compared with the pure WO_3 , but it possessed a greater limit of detection (>2 ppm). Shen et al. [18] reported that Fe and C co-doped WO_3 could detect the acetone level down to 0.2 ppm, but regrettably, the voltage signal of 2 ppm acetone is ~ 0.9 V while that of 0.9 ppm acetone is ~ 0.8 V, with the voltage signal increasing by only 13%, which tends to confuse diabetic patients and healthy controls. In addition, the poor selectivity of acetone restricted the further application of In_2O_3 nanobelts [19] and SnO_2 nanostructures [21]. At the same time, the high relative humidity ($\sim 75\%$) considerably reduced the response of the Pt-decorated In_2O_3 nanoparticles to acetone at ppm-level [20]. Therefore, superior response and high selectivity toward the trace concentration acetone at high humidity ($>80\%$) still remain great challenges in MOX gas sensors.

Our earlier reports [27–29] provided useful methods to enhance the response of MOX gas sensors. An n-type field effect transistor (FET) circuit has been proposed to amplify the apparent response of commercial sensor TGS 2602 (Figaro, Japan) [30] to toluene by around five times [27]. Besides this, the other commercial sensor, MP-4 sensor (Winsen, China) [31], in a coupling p+n FET circuit exhibits a ~ 14 -fold higher apparent response to 150 ppm methane than that in the traditional circuit [29]. In this paper, a novel interlocking p+n FET amplification circuit is designed for Mn-doped ZnO nanoparticles (MZO) in order to detect acetone at low concentrations, especially at 2 ppm. The MZO in this interlocking p+n FET circuit shows a transient response (voltage signal of 4.0 V) to 2 ppm acetone, whereas the response to the acetone lower than 2 ppm is negligible (voltage signal of <0.3 V). In other words, the response realizes a jump at the 2 ppm acetone, which is suitable for the qualitative detection of diabetes.

2. Design Scheme of the Amplification Circuit

Figure 1 illustrates the circuit for MZO sensor which is developed from the traditional circuit to the interlocking p+n FET circuit. To begin with, the MZO sensor (R_S) is connected in series with the load resistance (R_L) when V_{CC} of 5 V is applied in the traditional circuit. The part voltage of R_L is the output voltage (V_{OUT}). R_S of MZO (~ 95 M Ω) is much larger than R_L (~ 7 M Ω) to make the V_{OUT} as low as ~ 0.4 V, namely the baseline in air. When MZO is exposed to the acetone, R_S will decrease and the current will increase, inducing the growth of V_{OUT} in the acetone. Briefly, the change of R_S is the only factor to affect the change of V_{OUT} in the traditional circuit.

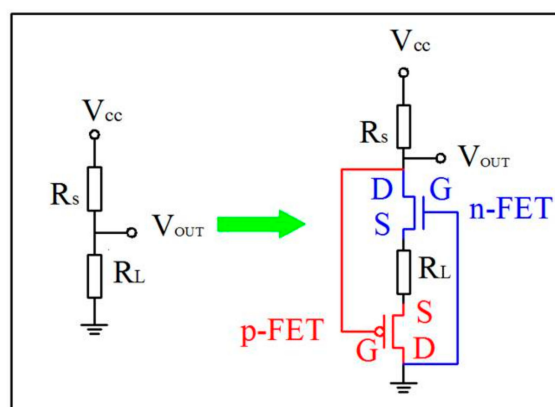


Figure 1. Design scheme of the traditional circuit and the interlocking p+n field effect transistor (FET) circuit for metal oxide (MOX) acetone sensor.

Then, an n-type and a p-type FETs are added into the circuit, forming the interlocking p+n circuit as shown in Figure 1. It is found that this circuit is different from the coupling or synergetic p+n circuits in Figure S1 in the supporting information according to our previous reports [28,29]. Similarly, the V_{OUT} is still low in air using the same R_L due to the negligible resistance of FET (R_{FET}) at ON state ($\sim 100 \Omega$). Acetone exposure leads to the decrease of R_S , followed by the growth of $|V_{GS}|$ of both FETs, making them work at OFF state ($\sim 1 \text{ G}\Omega$). Ultimately, the V_{OUT} grows large dramatically. In short, the V_{OUT} is under the double influence of R_S and R_{FET} in the interlocking p+n FET circuit.

3. Experimental

The MZO acetone sensor is homemade as mentioned earlier [32]. The TGS 2602 and MP-4 sensors are commercial gas sensors used to detect toluene and methane, respectively. The 2SJ103 (TOSHIBA, Tokyo, Japan) [33] is a p-type transistor and the 2SK544 (SANYO, Moriguchi, Japan) [34] and 2SK427 (SANYO, Japan) [35] are the n-type transistors. The $I_{DS}-V_{GS}$ curves and $I_{DS}-V_{DS}$ curves of 2SK427 and 2SJ103 are obtained by the Keithley 4200 semiconductor analyzer (Lake shore cryotronics, Westerville, OH, USA). The sensing property of MZO is carried out on the static gas sensing test system Hanwei WS-30A (Winsen, Zhengzhou, China) [36–38] equipped with the load resistance card under the relative humidity, i.e., RH (25% and 85%), where RH is defined as the percentage of water vapor pressure in air versus saturated water vapor pressure at the same temperature. The p- and n-FETs purchased from the market are soldered onto the resistance card with D, S and G electrodes forming the interlocking p+n FET circuit as shown in Figure 1. Certain amounts of the 40 v/v% acetone solution were dropped with a micro syringe onto an evaporator in the test chamber (total volume 18 L) to generate different concentrations of acetone gas varying from 0.5 to 3 ppm. This method is also applicable for other gases, including formaldehyde, acetaldehyde, toluene and ethanol. All of the gases were tested at an operating temperature of 340 °C according to our previous report [32]. Then the commercial MP-4 and TGS 2602 MOX sensors were utilized to detect the methane and toluene by using the interlocking p+n FET circuit respectively. More details of their sensing property measurements are seen in the references [28,29]. For the traditional circuit and the interlocking p+n FET circuit, the voltage signal is defined as voltage difference in acetone and in air and the response time is defined as the time needed to reach the maximum voltage from baseline voltage.

4. Results and Discussion

4.1. Response and Selectivity to Acetone

The MZO material was synthesized by coprecipitation method as reported in our previous paper [32]. Typically, 50 mL ZnSO_4 and MnSO_4 aqueous solution was added drop-wisely into 100 mL NH_4HCO_3 solution, and the precipitation was rinsed and calcined at 500 °C for 2 h to get the product. The responses to acetone are measured from 200 °C to 370 °C, and the working temperature was optimized to be 340 °C and the doping concentration of Mn was optimized to be 2.2 mol %. In addition, the selectivity measurement illustrates that the response to acetone is much higher than those to ethanol, formaldehyde and benzene. This is due to the relatively higher surface acidity which prefers acetone adsorption and reaction. On the other side, if the surface is tuned to be more alkaline by CdO decoration, the response can be tuned to be higher to ethanol. In this study, only the MZO sensor is adopted for selective detection of acetone at the criteria concentration of 1–2 ppm for breath analysis. However, the voltage signals of MZO to 1 ppm and 2 ppm acetone are $\sim 0.3 \text{ V}$ and $\sim 0.4 \text{ V}$, with the voltage signal increasing by only 0.1 V. Thus, it is essential to enhance the voltage signal of MZO to the trace concentration of acetone in order to diagnose diabetes.

The output voltages of MZO sensor in the traditional electric circuit and the interlocking p+n FET circuit as a function of acetone concentrations between 0.5 and 3 ppm at 25% RH are shown in Figure 2. It is obvious that MZO sensors in both the interlocking p+n FET and the traditional circuits exhibit an almost equally small voltage signal ($< 0.3 \text{ V}$) to 0.5 and 1 ppm acetone while the former have

much higher voltage signals (>4.0 V) to 2 and 3 ppm acetone than the latter (~ 0.5 V). It is found that the interlocking p+n FET circuit makes MZO realize a response jump at 2 ppm acetone, and thus the 2 ppm is named as the jump point of acetone. Figure 2 also illustrates that the output voltage of the traditional circuit has recovered to baseline when air was reinjected into the gas chamber. However, the V_{OUT} of the interlocking p+n FET circuit still remains at ~ 4.5 V for a long time. To recover the baseline, the power is turned off for ~ 5 s and then turned on again.

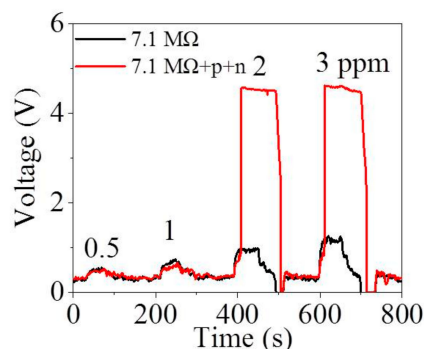


Figure 2. Output voltage of Mn-doped ZnO (MZO) to acetone from 0.5 to 3 ppm in the traditional electric circuit and the interlocking p+n FET circuit (R_L is 7.1 M Ω) under a humidity of 25%.

The selectivity of the MZO sensor is taken into consideration. The response of MZO sensors to other species of VOCs, including formaldehyde, acetaldehyde, toluene and ethanol, is shown in Figure 3a–d. Taking the formaldehyde gas, for instance, the MZO sensor in this interlocking p+n FET circuit displays a transient response (voltage signal of ~ 4.0 V) to 160 ppm formaldehyde while it responds a little (voltage signal of ~ 0.5 V) to formaldehyde lower than 160 ppm in Figure 3a. Other species of VOCs share the same feature. Figure 3a–d shows 160 ppm, 2000 ppm, 400 ppm and 4 ppm are the jump points of formaldehyde, acetaldehyde, toluene and ethanol, respectively, indicating that the MZO sensor in the interlocking p+n FETs circuit has excellent selectivity to acetone. Moreover, it is clear that the smallest gap exists between the jump points of ethanol and acetone, suggesting that the ethanol is likely to interfere with the acetone detection thus leading to the false diagnosis of the diabetes. Fortunately, many studies show that the ethanol level in the exhaled gas of healthy humans is found to be 770 ppb [39] or even lower [40,41], little affecting the acetone detection.

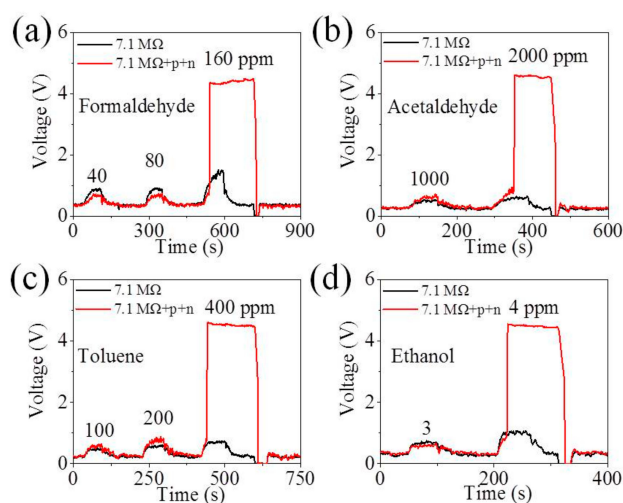


Figure 3. Output voltage of Mn-doped ZnO (MZO) to (a) formaldehyde from 40 to 160 ppm and (b) acetaldehyde from 1000 to 2000 ppm; (c) toluene from 100 to 400 ppm (d) ethanol from 3 to 4 ppm in the traditional circuit and the interlocking p+n FET circuit (R_L is 7.1 M Ω) under humidity of 25%.

4.2. Acetone Detection under 85% Humidity

More importantly, the relative humidity of the exhaled breath is higher than 80% RH at 1 atm and 25 °C [42], which has a negative effect on sensing performance such as water vapor poisoning [43]. Thus, we perform the gas detection of acetone under 85% humidity to investigate the potential feasibility of MZO sensors in the interlocking p+n FET for diagnosis of diabetes as shown in Figure 4a. In the present work, MZO sensors in the interlocking p+n FET are free from the influence of the high humidity and maintain a transient response to 2 ppm acetone. In addition, the response to 2 ppm acetone is ~4.0 V while that of 1 ppm acetone is ~0.3 V. The response is increased by 3.7 V (1233%), much higher than those in the references [18,38,44,45], making it easy to sort out qualitatively diabetic patients from normal people. According to Figure 4a, the baseline voltage in air is ~0.5 V and the maximum voltage in 2 ppm acetone is ~4.5 V, therefore it needs a response time of ~17 s to change from ~0.5 V to ~4.5 V, faster compared with many published results [11,12,26,46]. In addition, ~340 °C is a common heating temperature for metal oxide MOX gas sensors to detect the acetone, which further diagnose the diabetes [10,26,46,47].

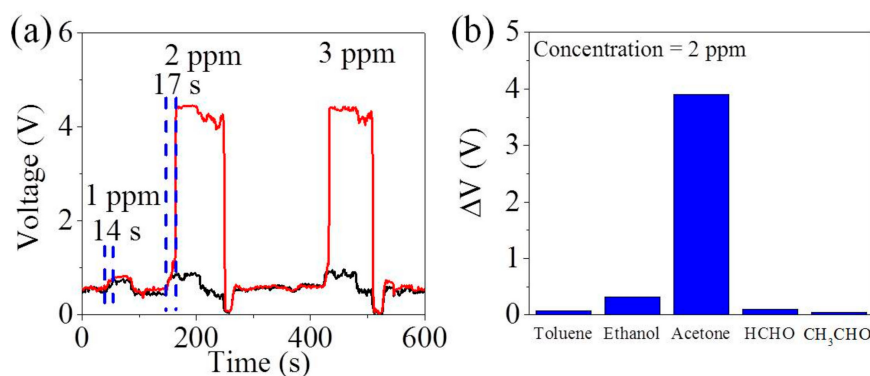


Figure 4. (a) Output voltage of MZO to acetone from 1 to 3 ppm in the traditional circuit and the interlocking p+n FET circuit (R_L is 7.1 MΩ) in the humid atmosphere of 85%; (b) The change of output voltage (ΔV) to different gases at 2 ppm (RH = 85%) for MZO in the interlocking p+n FET circuit (R_L is 7.1 MΩ).

Similarly, five species gases (acetone, ethanol formaldehyde, acetaldehyde and toluene) at 2 ppm are tested to further prove the selectivity of MZO sensors in the interlocking p+n FET circuit at the relative humidity of 85% shown Figure 4b, where it is clear that the voltage signal (ΔV) of acetone is much higher than those of other species of gases. Besides, it is worthwhile to note that formaldehyde, a biomarker of breast cancer, is measured as 0.45–1.20 ppm exhaled from people suffering from breast cancer [5]. In addition, several VOCs including acetaldehyde and toluene appeared at levels of 10–20 ppb in normal people's breath, whereas they are elevated to 10–100 ppb for lung cancer patients [7,8,48]. Therefore, diabetes diagnosis using MZO in this interlocking p+n FET circuit is able to exclude interference from breast cancer and lung cancer.

As to the expense, the cost increased by the two FETs in this interlocking circuit is only around 10% of the gas sensor. Moreover, this interlocking circuit enjoys the flexibility in the matching of p- and n-FETs compared to the synergetic p+n FET circuit with the restriction on the working curves of the FET [28]. In the meanwhile, MZO sensors in the interlocking p+n FET cannot be sensitive to the gas exhaled by the normal people. On the contrary, it outputs a high voltage signal (~4.0 V) exposed to the gas exhaled by the diabetes patients (generally 1.8–10 ppm [49]), in favor of the widespread and low cost screening of the diabetes.

4.3. Universality of the Interlocking p+n FET Circuit

To further prove the universality of this interlocking p+n FET circuit, the commercial MOX sensors MP-4 (Winsen, China) [31] and TGS 2602 (Figaro, Osaka, Japan) [30] are carried on the gas sensing property measurement at the relative humidity of 25%.

Figure 5a shows that 100 ppm is the jump point of methane when MP-4 sensors are placed in the interlocking circuit. As we all know, the lower explosion limit (LEL) of methane is approximately 50,000 ppm [50], and hence, MP-4 sensors can be used to detect the trace concentration of methane to avoid accidental explosion. Figure 5b illustrates that TGS 2602 sensor in this interlocking circuit produces the transient response to 0.25 ppm toluene while it exhibits a tiny response to toluene lower than 0.25 ppm. According to the vehicle indoor air quality (VIAQ), 1.0 mg/m³ (0.26 ppm) is the maximum permitted limit of toluene in indoor air of a car. Thus, this p+n FET circuit entitles TGS 2602 to detect whether the concentration of toluene is beyond this standard value. In all, this interlocking p+n FET circuit is extensively applicable to MOX gas sensors.

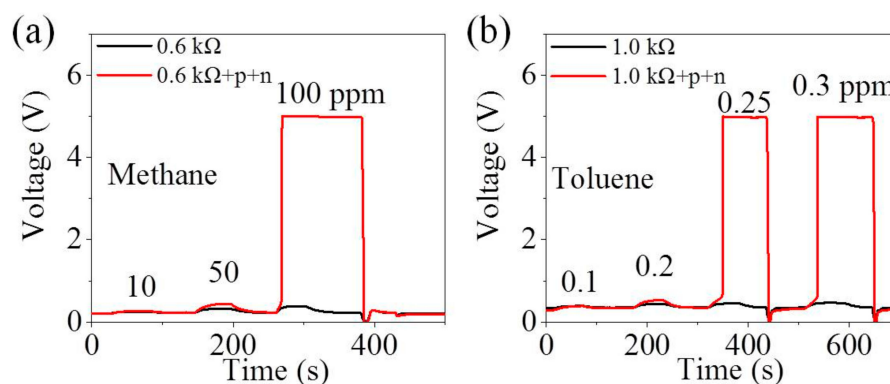


Figure 5. Output voltage of (a) MP-4 to methane from 10 to 100 ppm and (b) TGS 2602 to toluene from 0.1 to 0.3 ppm in the traditional circuit and the interlocking p+n FET circuit under humidity of 25%.

4.4. Amplification Mechanism of the Interlocking p+n FET Circuit

In the earlier reports [27], the amplification effect of 2SK544 is due to the tiny change of the gate voltage inducing a dramatic resistance change of 2SK544. Thus, the mechanism of the interlocking p+n FET circuit is investigated from the perspective of the amplification effect of FET.

The black solid line in Figure 6 represents the curve of n-type FET amplification circuit with R_L of 7.1 M Ω . The blue dash line is the fitting curve of many maximum points from the curves of n-type FET amplification circuit using different R_L , more details are seen in Figure S4. The violet, and green solid lines in Figure 6 are expressed respectively as

$$R_L + R_{FET, air} = V_{CC}/I - R_{S, air} \quad (1)$$

$$R_L + R_{FET, 2 ppm} = V_{CC}/I - R_{S, 2 ppm} \quad (2)$$

where V_{CC} is the applied voltage (5 V), $R_{FET, air}$ and $R_{FET, 2 ppm}$ represent FET resistance in air and 2 ppm acetone respectively. $R_{S, air}$ and $R_{S, 2 ppm}$ are the MZO sensor resistance (R_S) in air and 2 ppm acetone individually. $R_{S, air}$ and $R_{S, 2 ppm}$ are experimentally measured as 95 M Ω and 36 M Ω respectively.

According to the interlocking p+n FET circuit in Figure 1, the following formulas can be obtained:

$$-V_{GS(n)} = I \times R_L - V_{DS(p)} \quad (3)$$

$$V_{GS(p)} = I \times R_L + V_{DS(n)} \quad (4)$$

$$V_{OUT} = -V_{GS(n)} + V_{DS(n)} \quad (5)$$

where $V_{GS(p)}$ and $V_{DS(p)}$ are V_{GS} and V_{DS} of 2SJ103 respectively. $V_{GS(n)}$ and $V_{DS(n)}$ are V_{GS} and V_{DS} of 2SK427 respectively. I represents the circuit current.

The formula of the working curve of the interlocking p+n FET circuit can be obtained from Formulas (3)–(5).

$$R_{FET} = V_{DS(n)}/I - V_{DS(p)}/I \quad (6)$$

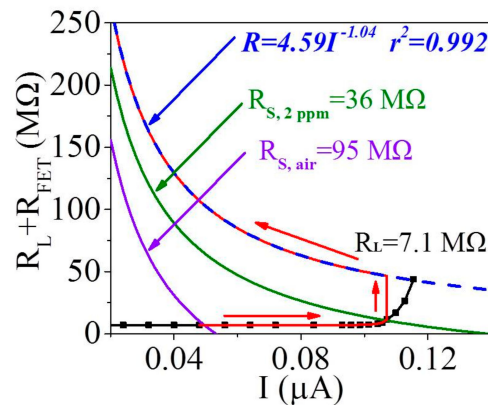


Figure 6. The approximate curve of interlocking p+n FET circuit with R_L of 7.1 MΩ (red solid curve). The blue dash curve is the fitting curve of the maximum points from five solid curves of n-type FET 2SK427 circuit with R_L 7.1, 10, 20, 30 and 50 MΩ respectively. And the fitting curve formula is $R=4.59I^{-1.04}$ ($r^2=0.992$).

$V_{DS(n)}$ is under the double effect of V_{GS} of two FETs, and so is $V_{DS(p)}$. Thus, both $V_{DS(n)}$ and $V_{DS(p)}$ are difficult to analyze and there is a tight interplay between 2SK427 and 2SJ103 in terms of the amplification effect, just as described in Formulas (3) and (4). Therefore, it is essential to simplify, approximate and estimate the working curve of the interlocking p+n FET circuit. This is divided into three stages:

- The first stage is in clean air. Both FETs work at ON state, so their resistances can be neglected compared to 7.1 MΩ. Therefore, this interlocking circuit in clean air is equivalent to the traditional circuit, denoted by the intersection of the black and violet solid lines seen in Figure 6;
- Introducing a trace concentration (<2 ppm) of acetone gas into the gas chamber is the second stage. The limited V_{OUT} amplification is generated by 2SK427 while 2SJ103 is still at ON state. Thus, this interlocking p+n FET circuit is equivalent to the single n-type FET circuit, i.e., $R_L + R_{FET} = (V_{DS(n)} + V_{GS(n)})/I$, whose curve overlaps the curve of the single n-type FET circuit with R_L of 7.1 MΩ (black solid line) shown in Figure 6;
- More than 2 ppm acetone gas is introduced in the third stage. Both 2SK427 and 2SJ103 tend to work at OFF state, whose resistances can arrive at 10 GΩ level. This stage is quite complex, thus the starting and ending points of this stage need to be determined for the sake of simplicity. It is obvious that the starting point is exactly the intersection (0.11 μA, 11 MΩ) of both the black and green lines in Figure 6. As to the ending point, its calculation is elaborated in the following part.

At the ending point of the third stage, two FETs are hypothesized to be at OFF state, so the circuit current decreases by 2–3 orders of magnitude. Therefore, Formulas (3) and (4) are simplified as below:

$$V_{GS(n)} = V_{DS(p)} \quad (7)$$

$$V_{GS(p)} = V_{DS(n)} \quad (8)$$

On the basis of Formulas (7) and (8) and V_{DS} - I_{DS} curves of n-type 2SK427 and p-type 2SJ103 in Figure S2, $V_{GS(n)}$, $V_{DS(n)}$, $V_{GS(p)}$ and $V_{DS(p)}$ is calculated as -1.3 V, 3.7 V, 3.7 V and -1.3 V individually. The threshold voltages (V_T) of 2SK427 and 2SJ103 are -0.6 V and 1.2 V respectively according to Figure S3, and hence $V_{GS(n)}$ of -1.3 V and $V_{GS(p)}$ of 3.7 V are large enough to turn of the FET to support reliability of hypothesis above. Furthermore, the minimum circuit current (I_{min}) is calculated as 1.7×10^{-4} μ A from the point where $V_{GS(n)} = -1.3$ V and $V_{DS(n)} = 3.7$ V in Figure S2a. Then I_{min} is substituted in the formula of blue dash line in Figure 6, the maximum resistance (R_{max}) is calculated as 3.9×10^4 M Ω . Therefore, the ending point of the third stage is denoted by the point (I_{min} , R_{max}), i.e., (1.7×10^{-4} μ A, 3.9×10^4 M Ω), not marked in Figure 6; more information is seen in Figure S4.

The working curve of the interlocking p+n FET circuit in the third stage is estimated. It starts with the point (0.11 μ A, 11 M Ω) and then increases almost vertically, very similarly to the coupling p+n FET circuit previous [29], followed by arriving at the ending point (1.7×10^{-4} μ A, 3.9×10^4 M Ω) along the blue dash line. The working curve of this interlocking p+n FET circuit including three stages is the red solid line in Figure 6 and Figure S4, where the resistance jump of FET is the basic reason why this interlocking circuit can produce the transilient response.

It is worthwhile to note that the theoretical value of V_{OUT} is ~ 5 V (3.7 V + 1.3 V) according to Formula (5) while the actual value is ~ 4.5 V seen from Figures 2–4, which can be explained by characteristics of the parallel circuit. From the circuit diagram in Figure 7a, R_{FET} and R_L are parallel with the voltmeter (~ 800 M Ω in Figure S5). R_{FET} and R_L in air are much smaller compared to the resistance of the voltmeter (R_V), hence circuit 1 is closed in Figure 7a. However, both values of R_{FET} in 2 ppm acetone are much larger than R_V . Thus, circuit 1 is open while circuit 2 is closed in Figure 7a and V_{OUT} is calculated to be ~ 4.5 V. Briefly, this interlocking p+n FET circuit can be switched between circuit 1 and 2, as shown in Figure 7b. Consequently, the interlocking p+n FET amplification circuit can serve as a novel technology for enhanced response to breath biomarkers and offer a potential platform for application in diabetes diagnosis.

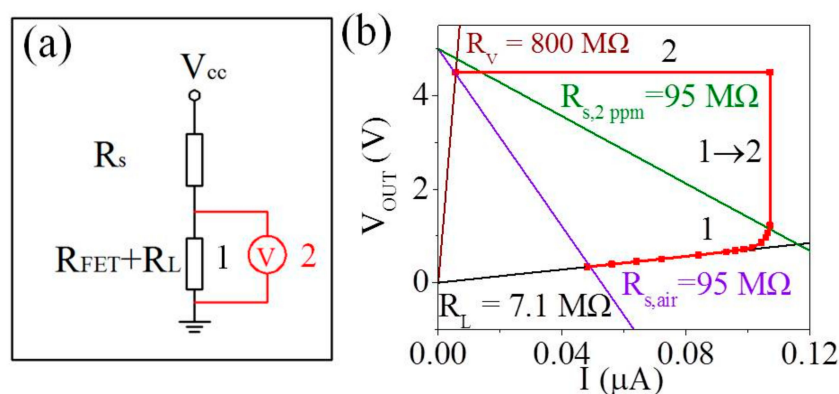


Figure 7. (a) Circuit schematic of the static gas sensing test system (b) The approximate output voltage of the interlocking p+n FET circuit with R_L of 7.1 M Ω (red solid curve).

5. Conclusions

In summary, a simple interlocking p+n FET circuit has successfully enhanced the response of MZO to acetone. It is interesting that a superior detecting capacity of MZO in this interlocking circuit with a transilient response (voltage signal of ~ 4.0 V) was obtained at ≥ 2 ppm acetone gas under high relative humidity of 85%, whereas it is trivial (~ 0.3 V) for acetone gas lower than 2 ppm. This response difference ($\sim 1233\%$) is high enough to satisfy the requirements for distinguishing diabetic patients from examinees. In addition, this technology also possesses a better acetone selectivity against formaldehyde, acetaldehyde, toluene and ethanol. Moreover, rapid response (~ 17 s) is appropriate to the breath analysis and the increased cost of this interlocking circuit is mainly the expense of the two FETs, about 10% of the gas sensor. Furthermore, this interlocking circuit can be directly utilized in other MOX gas

sensors to detect the target gases. The transient response of MOX sensor in the interlocking circuit is likely due to the jump of FET resistance induced by their gate voltage. These results demonstrate the promise for the qualitative detection of biomarker molecules in breath. Many efforts will be made to fabricate practical exhaled breath detecting sensors by employing the concepts in this study.

Supplementary Materials: The following are available online at <http://www.mdpi.com/1424-8220/18/6/1914/s1>, Figure S1: The differences among the synergetic, coupling and interlocking p+n FET circuit for MOX acetone sensor, Figure S2: (a) V_{DS} - I_{DS} curves of FET 2SK427, V_{GS} changes from -5 V to 0 V (step is 0.1 V). (b) V_{DS} - I_{DS} curves of FET 2SJ103, V_{GS} changes from 0 V to 5 V (step is 0.1 V), Figure S3: I_{DS} - V_{GS} curves of FETs 2SK427 (a) and 2SJ103 (b). (c) and (d) the calculation of V_T , Figure S4: The approximate curve of interlocking p+n FET circuit with R_L of 7.1 M Ω (red solid curve). The blue dash curve is the fitting curve of the maximum points from five solid curves of n-type FET 2SK427 circuit with R_L 7.1 , 10 , 20 , 30 and 50 M Ω respectively. The fitting curve formula is $R = 4.59 I^{-1.04}$ ($r^2 = 0.992$), Figure S5: (a) Output voltage of Mn doped ZnO (MZO) in the traditional circuit and the interlocking p+n FET circuit with R_L ON or OFF. (b) Circuit schematic of the static gas sensing test system.

Author Contributions: X.Z. proposed the idea, analyzed data and wrote the paper. The MZO sensing material was fabricated by J.W. Gas sensing property measurement was performed by X.Z. and Z.W., N.H., Y.W. and Y.B. contributed the analysis of the results. N.H. contributed the final revision of this paper. N.H. and Y.C. directed the research as the principal investigator (PI) of the project.

Funding: This research was funded by the National Key R&D Program of China (2016YFC0207100), the National Natural Science Foundation of China (51272253), Guangdong Innovative and Entrepreneurial Research Team Program (No. 2014ZT05C146), and the State Key Laboratory of Multiphase Complex Systems (MPCS-2014-C-01).

Conflicts of Interest: The authors declare no conflict of interest.

References

- Haick, H.; Broza, Y.Y.; Mochalski, P.; Ruzsanyi, V.; Amann, A. Assessment, origin, and implementation of breath volatile cancer markers. *Chem. Soc. Rev.* **2014**, *43*, 1423–1449. [[CrossRef](#)] [[PubMed](#)]
- Moon, H.G.; Jung, Y.; Han, S.D.; Shim, Y.S.; Shin, B.; Lee, T.; Kim, J.S.; Lee, S.; Jun, S.C.; Park, H.H.; et al. Chemiresistive Electronic Nose toward Detection of Biomarkers in Exhaled Breath. *ACS Appl. Mater. Interfaces* **2016**, *8*, 20969–20976. [[CrossRef](#)] [[PubMed](#)]
- Jang, J.-S.; Choi, S.-J.; Kim, S.-J.; Hakim, M.; Kim, I.-D. Rational Design of Highly Porous SnO₂ Nanotubes Functionalized with Biomimetic Nanocatalysts for Direct Observation of Simulated Diabetes. *Adv. Funct. Mater.* **2016**, *26*, 4740–4748. [[CrossRef](#)]
- Blanchet, L.; Smolinska, A.; Baranska, A.; Tigchelaar, E.; Swertz, M.; Zhernakova, A.; Dallinga, J.W.; Wijmenga, C.; van Schooten, F.J. Factors that influence the volatile organic compound content in human breath. *J. Breath Res.* **2017**, *11*, 016013. [[CrossRef](#)] [[PubMed](#)]
- Ebeler, S.E.; Clifford, A.J.; Shibamoto, T. Quantitative analysis by gas chromatography of volatile carbonyl compounds in expired air from mice and human. *J. Chromatogr. B* **1997**, *702*, 211–215. [[CrossRef](#)]
- Van den Velde, S.; Nevens, F.; Van Hee, P.; van Steenberghe, D.; Quirynen, M. GC-MS analysis of breath odor compounds in liver patients. *J. Chromatogr. B* **2008**, *875*, 344–348. [[CrossRef](#)] [[PubMed](#)]
- Smith, D.; Wang, T.; Sule-Suso, J.; Spanel, P.; El Haj, A. Quantification of acetaldehyde released by lung cancer cells in vitro using selected ion flow tube mass spectrometry. *Rapid Commun. Mass Spectrom.* **2003**, *17*, 845–850. [[CrossRef](#)] [[PubMed](#)]
- Poli, D.; Carboognani, P.; Corradi, M.; Goldoni, M.; Acampa, O.; Balbi, B.; Bianchi, L.; Rusca, M.; Mutti, A. Exhaled volatile organic compounds in patients with non-small cell lung cancer: Cross sectional and nested short-term follow-up study. *Respir. Res.* **2005**, *6*, 71. [[CrossRef](#)] [[PubMed](#)]
- Shin, J.; Choi, S.-J.; Lee, I.; Youn, D.-Y.; Park, C.O.; Lee, J.-H.; Tuller, H.L.; Kim, I.-D. Thin-Wall Assembled SnO₂ Fibers Functionalized by Catalytic Pt Nanoparticles and their Superior Exhaled-Breath-Sensing Properties for the Diagnosis of Diabetes. *Adv. Funct. Mater.* **2013**, *23*, 2357–2367. [[CrossRef](#)]
- Xing, R.; Li, Q.; Xia, L.; Song, J.; Xu, L.; Zhang, J.; Xie, Y.; Song, H. Au-modified three-dimensional In₂O₃ inverse opals: Synthesis and improved performance for acetone sensing toward diagnosis of diabetes. *Nanoscale* **2015**, *7*, 13051–13060. [[CrossRef](#)] [[PubMed](#)]
- Righettoni, M.; Tricoli, A.; Pratsinis, S.E. Si:WO₃ Sensors for Highly Selective Detection of Acetone for Easy Diagnosis of Diabetes by Breath Analysis. *Anal. Chem.* **2010**, *82*, 3581–3587. [[CrossRef](#)] [[PubMed](#)]

12. Choi, S.J.; Lee, I.; Jang, B.H.; Youn, D.Y.; Ryu, W.H.; Park, C.O.; Kim, I.D. Selective diagnosis of diabetes using Pt-functionalized WO₃ hemitube networks as a sensing layer of acetone in exhaled breath. *Anal. Chem.* **2013**, *85*, 1792–1796. [[CrossRef](#)] [[PubMed](#)]
13. Smith, D.; Wang, T.; Spanel, P. On-line, simultaneous quantification of ethanol, some metabolites and water vapour in breath following the ingestion of alcohol. *Physiol. Meas.* **2002**, *23*, 477–489. [[CrossRef](#)] [[PubMed](#)]
14. Smith, D.; Spanel, P.; Fryer, A.A.; Hanna, F.; Ferns, G.A. Can volatile compounds in exhaled breath be used to monitor control in diabetes mellitus? *J. Breath Res.* **2011**, *5*, 022001. [[CrossRef](#)] [[PubMed](#)]
15. Deng, C.; Zhang, J.; Yu, X.; Zhang, W.; Zhang, X. Determination of acetone in human breath by gas chromatography-mass spectrometry and solid-phase microextraction with on-fiber derivatization. *J. Chromatogr. B* **2004**, *810*, 269–275. [[CrossRef](#)]
16. Ueta, I.; Saito, Y.; Hosoe, M.; Okamoto, M.; Ohkita, H.; Shirai, S.; Tamura, H.; Jinno, K. Breath acetone analysis with miniaturized sample preparation device: In-needle preconcentration and subsequent determination by gas chromatography-mass spectroscopy. *J. Chromatogr. B* **2009**, *877*, 2551–2556. [[CrossRef](#)] [[PubMed](#)]
17. Kaur, J.; Anand, K.; Kaur, A.; Singh, R.C. Sensitive and selective acetone sensor based on Gd doped WO₃ /reduced graphene oxide nanocomposite. *Sens. Actuators B Chem.* **2018**, *258*, 1022–1035. [[CrossRef](#)]
18. Shen, J.-Y.; Wang, M.-D.; Wang, Y.-F.; Hu, J.-Y.; Zhu, Y.; Zhang, Y.X.; Li, Z.-J.; Yao, H.-C. Iron and carbon codoped WO₃ with hierarchical walnut-like microstructure for highly sensitive and selective acetone sensor. *Sens. Actuators B Chem.* **2018**, *256*, 27–37. [[CrossRef](#)]
19. Li, Y.; Xu, J.; Chao, J.; Chen, D.; Ouyang, S.; Ye, J.; Shen, G. High-aspect-ratio single-crystalline porous In₂O₃ nanobelts with enhanced gas sensing properties. *J. Mater. Chem.* **2011**, *21*, 12852–12857. [[CrossRef](#)]
20. Karmaoui, M.; Leonardi, S.G.; Latino, M.; Tobaldi, D.M.; Donato, N.; Pullar, R.C.; Seabra, M.P.; Labrincha, J.A.; Neri, G. Pt-decorated In₂O₃ nanoparticles and their ability as a highly sensitive (<10 ppb) acetone sensor for biomedical applications. *Sens. Actuators B Chem.* **2016**, *230*, 697–705. [[CrossRef](#)]
21. Li, Y.X.; Guo, Z.; Su, Y.; Jin, X.B.; Tang, X.H.; Huang, J.R.; Huang, X.J.; Li, M.Q.; Liu, J.H. Hierarchical Morphology-Dependent Gas-Sensing Performances of Three-Dimensional SnO₂ Nanostructures. *ACS Sens.* **2017**, *2*, 102–110. [[CrossRef](#)] [[PubMed](#)]
22. Wang, M.; Shen, Z.; Chen, Y.; Zhang, Y.; Ji, H. Atomic structure-dominated enhancement of acetone sensing for a ZnO nanoplate with highly exposed (0001) facet. *CrystEngComm* **2017**, *19*, 6711–6718. [[CrossRef](#)]
23. Alali, K.T.; Liu, J.; Liu, Q.; Li, R.; Zhang, H.; Aljebawi, K.; Liu, P.; Wang, J. Enhanced acetone gas sensing response of ZnO/ZnCo₂O₄ nanotubes synthesized by single capillary electrospinning technology. *Sens. Actuators B Chem.* **2017**, *252*, 511–522. [[CrossRef](#)]
24. Liu, C.; Wang, B.; Liu, T.; Sun, P.; Gao, Y.; Liu, F.; Lu, G. Facile synthesis and gas sensing properties of the flower-like NiO-decorated ZnO microstructures. *Sens. Actuators B Chem.* **2016**, *235*, 294–301. [[CrossRef](#)]
25. Wang, L.; Teleki, A.; Pratsinis, S.E.; Gouma, P.I. Ferroelectric WO₃ Nanoparticles for Acetone Selective Detection. *Chem. Mater.* **2008**, *20*, 4794–4796. [[CrossRef](#)]
26. Moon, H.G.; Jung, Y.; Jun, D.; Park, J.H.; Chang, Y.W.; Park, H.H.; Kang, C.Y.; Kim, C.; Kaner, R.B. Hollow Pt-Functionalized SnO₂ Hemipill Network Formation Using a Bacterial Skeleton for the Noninvasive Diagnosis of Diabetes. *ACS Sens.* **2018**, *3*, 661–669. [[CrossRef](#)] [[PubMed](#)]
27. Zhou, X.; Wang, Y.; Wang, J.; Xie, Z.; Wu, X.; Han, N.; Chen, Y. Amplifying the Signal of Metal Oxide Gas Sensors for Low Concentration Gas Detection. *IEEE Sens. J.* **2017**, *17*, 2841–2847. [[CrossRef](#)]
28. Zhou, X.; Wang, Y.; Wang, Z.; Yang, L.; Wu, X.; Han, N.; Chen, Y. Synergetic p+n Field-Effect Transistor Circuits for ppb-Level Xylene Detection. *IEEE Sens. J.* **2018**, *18*, 3875–3882. [[CrossRef](#)]
29. Zhou, X.; Yang, L.; Bian, Y.; Ma, X.; Han, N.; Chen, Y. Coupling p+n Field-Effect Transistor Circuits for Low Concentration Methane Gas Detection. *Sensors* **2018**, *18*, 787. [[CrossRef](#)] [[PubMed](#)]
30. Apollo Union. Available online: <http://www.apollounion.com/download.asp?filename=Upload/DownFiles/2602tgs.pdf> (accessed on 1 June 2018).
31. WinsenTool MP-4. Available online: http://style.winsensor.com/pro_pdf/MP-4.pdf (accessed on 1 June 2018).
32. Wang, J.; Yang, J.; Han, N.; Zhou, X.; Gong, S.; Yang, J.; Hu, P.; Chen, Y. Highly sensitive and selective ethanol and acetone gas sensors based on modified ZnO nanomaterials. *Mater. Des.* **2017**, *121*, 69–76. [[CrossRef](#)]
33. TOSHIBA Field Effect Transistor. Available online: http://www.ic37.com/TOSHIBA/2SJ103_datasheet_4565374/ (accessed on 1 June 2018).

34. Sanyo 2SK544. Available online: http://www.ic37.com/SANYO/2SK544_datasheet_639966/ (accessed on 1 June 2018).
35. Sanyo 2SK427. Available online: http://www.ic37.com/SANYO/2SK427_datasheet_639960/ (accessed on 1 June 2018).
36. Qin, N.; Wang, X.H.; Xiang, Q.; Xu, J.Q. A biomimetic nest-like ZnO: Controllable synthesis and enhanced ethanol response. *Sens. Actuators B Chem.* **2014**, *191*, 770–778. [[CrossRef](#)]
37. Wang, X.-j.; Wang, W.; Liu, Y.-L. Enhanced acetone sensing performance of Au nanoparticles functionalized flower-like ZnO. *Sens. Actuators B Chem.* **2012**, *168*, 39–45. [[CrossRef](#)]
38. Shen, J.-Y.; Zhang, L.; Ren, J.; Wang, J.-C.; Yao, H.-C.; Li, Z.-J. Highly enhanced acetone sensing performance of porous C-doped WO₃ hollow spheres by carbon spheres as templates. *Sens. Actuators B Chem.* **2017**, *239*, 597–607. [[CrossRef](#)]
39. Fenske, J.D.; Paulson, S.E. Human Breath Emissions of VOCs. *J. Air Waste Manag. Assoc.* **2011**, *49*, 594–598. [[CrossRef](#)]
40. Conkle, J.P.; Camp, B.J.; Welch, B.E. Trace Composition of Human Respiratory Gas. *Arch. Environ. Health Int. J.* **1975**, *30*, 290–295. [[CrossRef](#)]
41. Galassetti, P.R.; Novak, B.; Nemet, D.; Rose-Gottron, C.; Cooper, D.M.; Meinardi, S.; Newcomb, R.; Zaldivar, F.; Blake, D.R. Breath Ethanol and Acetone as Indicators of Serum Glucose Levels: An Initial Report. *Diabetes Technol. Ther.* **2005**, *7*, 15–23. [[CrossRef](#)] [[PubMed](#)]
42. Xing, R.Q.; Xu, L.; Song, J.; Zhou, C.Y.; Li, Q.L.; Liu, D.L.; Song, H.W. Preparation and Gas Sensing Properties of In₂O₃/Au Nanorods for Detection of Volatile Organic Compounds in Exhaled Breath. *Sci. Rep.* **2015**, *5*, 10717. [[CrossRef](#)] [[PubMed](#)]
43. Ma, N.; Suematsu, K.; Yuasa, M.; Kida, T.; Shimano, K. Effect of water vapor on Pd-loaded SnO₂ nanoparticles gas sensor. *ACS Appl. Mater. Interfaces* **2015**, *7*, 5863–5869. [[CrossRef](#)] [[PubMed](#)]
44. Xiao, T.; Wang, X.-Y.; Zhao, Z.-H.; Li, L.; Zhang, L.; Yao, H.-C.; Wang, J.-S.; Li, Z.-J. Highly sensitive and selective acetone sensor based on C-doped WO₃ for potential diagnosis of diabetes mellitus. *Sens. Actuators B Chem.* **2014**, *199*, 210–219. [[CrossRef](#)]
45. Umar, A.; Alshahrani, A.A.; Algarni, H.; Kumar, R. CuO nanosheets as potential scaffolds for gas sensing applications. *Sens. Actuators B Chem.* **2017**, *250*, 24–31. [[CrossRef](#)]
46. Kim, S.J.; Choi, S.J.; Jang, J.S.; Kim, N.H.; Hakim, M.; Tuller, H.L.; Kim, I.D. Mesoporous WO₃ Nanofibers with Protein-Templated Nanoscale Catalysts for Detection of Trace Biomarkers in Exhaled Breath. *ACS Nano* **2016**, *10*, 5891–5899. [[CrossRef](#)] [[PubMed](#)]
47. Kim, K.-H.; Kim, S.-J.; Cho, H.-J.; Kim, N.-H.; Jang, J.-S.; Choi, S.-J.; Kim, I.-D. WO₃ nanofibers functionalized by protein-templated RuO₂ nanoparticles as highly sensitive exhaled breath gas sensing layers. *Sens. Actuators B Chem.* **2017**, *241*, 1276–1282. [[CrossRef](#)]
48. Peng, G.; Tisch, U.; Adams, O.; Hakim, M.; Shehada, N.; Broza, Y.Y.; Billan, S.; Abdah-Bortnyak, R.; Kuten, A.; Haick, H. Diagnosing lung cancer in exhaled breath using gold nanoparticles. *Nat. Nanotechnol.* **2009**, *4*, 669–673. [[CrossRef](#)] [[PubMed](#)]
49. Park, S. Acetone gas detection using TiO₂ nanoparticles functionalized In₂O₃ nanowires for diagnosis of diabetes. *J. Alloys Compd.* **2017**, *696*, 655–662. [[CrossRef](#)]
50. Vuong, N.M.; Hieu, N.M.; Hieu, H.N.; Yi, H.; Kim, D.; Han, Y.-S.; Kim, M. Ni₂O₃-decorated SnO₂ particulate films for methane gas sensors. *Sens. Actuators B Chem.* **2014**, *192*, 327–333. [[CrossRef](#)]

